Measurement 240 (2025) 115652

Contents lists available at ScienceDirect

Measurement

journal homepage: www.elsevier.com/locate/measurement

Innovative surface acoustic wave devices: A solution for real time monitoring and self-cleaning cascade impactor

G. Fawaz *, FE. Dbibih, M. Vanotti, V. Soumann, V. Blondeau-Patissier

Université de Franche-Comté, CNRS, FEMTO-ST (UMR 6174), SupMicrotech ENSMM, 26 rue de l'Épitaphe, 25030 Besançon Cedex, France

ARTICLE INFO

Keywords:
Cascade impactor
SAW sensors
Lithium Niobate
Lithium Tantalate
Quartz
Particulate matter
PM10
PM2.5
POI
Electromechanical coupling coefficient
Thermal stability

ABSTRACT

This paper presents a comparative study of three types of surface acoustic waves sensors used for particulate matter detection along with a theoretical study tackling the possibility to switch to innovative materials called Piezoelectric-on-Insulator. These sensors are placed in a cascade impactor as impaction plates. Monitoring their phase variation allows us to measure the quantity of fine particles present in the air with high accuracy. Until now, the sensors used in our prototype are built on quartz substrate and present a sufficient sensitivity to fine particles. One major concern in our application is the fouling of the sensor's surface with particles upon long periods of exposure. This shaped our drive to develop a self-cleaning sensor relying on other substrates with stronger electromechanical coupling coefficient (k^2) [1]. Hence, the aim of this study is to demonstrate the possibility of using strongly coupled modes on different piezoelectric substrates for an accurate PM detection. Among these, different POI substrates are considered to assess their physical and acoustic properties, especially in terms of k^2 and thermal stability, for further optimization enabling their exploitation in the self-cleaning system that is being developed.

1. Introduction

Nowadays, outdoor pollution is rising in all areas causing around 7 million premature deaths worldwide yearly, according to the World Health Organization [2], majorly due to particulate matter (PM) penetrating into human lungs. The toxicity of particles is directly linked to their size. The smaller are the particles the deeper they penetrate in the human lung. Exposure to PM2.5 and PM10 has a proven connection with death due to cardiovascular and respiratory diseases such as asthma, chronic obstructive pulmonary disease (COPD), pulmonary fibrosis, pneumonia, and lung cancer [3–5]. For these reasons, there is a great urge for continuous air monitoring to align with the health-based standards. SAW sensors are widely used in diverse sensing application such as biosensors [6], gas sensors [7], temperature sensors [8], humidity sensors [9] and light detectors [10,11]. Surface acoustic waves (SAW) technology has been also attracting attention for particles measurement [12,13].

Among the most used systems for PM measurements, we name the cascade impactor. Despite its good performance, this equipment does not provide real time measurements. The impaction plates should be weighed before and after sampling, which is quite inconvenient and time consuming. For that reason, our team attempted to equip the impaction plates with SAW sensors [14,15] to ensure real-time measurements. Regardless of the stage in question, prolonged exposures to particles causes progressive fouling of the sensor's' surface affecting their sensitivity that tends to decrease with time and triggering the need to develop an integrated regeneration system that does not require any dismantling of the impactor to ensure continuous reliable readings.

Melvin Paquit *et al.* [16] have shown in a previous study that the use of Rayleigh waves with a delay line based on 128° Y-cut $LiNbO_3$ substrate allows, due to their out-of-plane elliptical polarization, to significantly displace particles from the substrate's surface. The displacement is achieved by applying a radio-frequency signal with a power level higher than 30 dBm. For particles issued from a candle smoke, shown in Fig. 1, with an average diameter smaller than 2.5 μm, 30 s was a sufficient period to move the particles off the surface under a 30 dBm power. For particles of silicon carbide (SiC) smaller than 5 μm in Fig. 2, 20 s at 31 dBm were needed to successfully remove the particles. This was also seen in a study conducted by Brunet *et al.* who investigated the behavior of a water droplet depending on the amplitude of SAW used and

* Corresponding author.
E-mail addresses: ghida.fawaz@femto-st.fr (G. Fawaz), fe.dbibih@femto-st.fr (FE. Dbibih), meddy.vanotti@femto-st.fr (M. Vanotti), valerie.soumann@femto-st.fr (V. Soumann), virginie.blondeau@femto-st.fr (V. Blondeau-Patissier).

https://doi.org/10.1016/j.measurement.2024.115652
Received 27 February 2024; Received in revised form 1 July 2024; Accepted 1 September 2024
Available online 2 September 2024

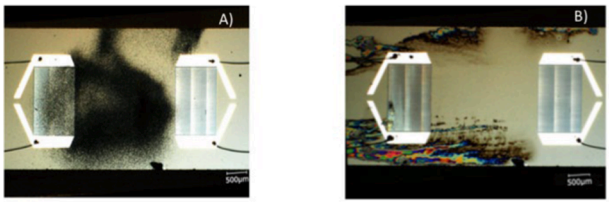

Fig. 1. View of SAW delay lines covered with particles smaller than 2.5 μm from a burning candle (A) before and (B) after high-power RF cleaning.

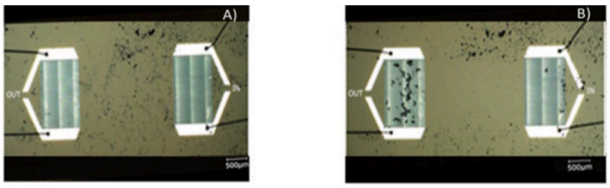

Fig. 2. View of SAW delay lines covered with particles smaller than 5 μm from SiC (A) before and (B) after high-power RF cleaning.

succeeded to displace it [17].

Moreover, to serve the goal of developing a cleaning system, superior mechanical and acoustic properties have been recently achieved by the use of innovative materials known as Piezoelectric-On-Insulator, denoted POI. These substrates are heterogeneous structures, obtained by mounting a thin layer of a piezoelectric material, namely lithium tantalate and lithium niobate, on an insulating layer of silicon with a layer of SiO_2 in between them. The technology behind it is called Smart-cut^{TM} technology consisting of ion implantation on a thick substrate to delaminate a thin layer. Through this process along with wafer bonding, the formation of stratified substrates of different materials is possible [18]. Knowing that lithium niobate and lithium tantalate in their bulk form present high thermal instability translated with negative temperature coefficients of frequency, the transition from bulk to POI has been proven to successfully target this factor, as discussed by Clairet *et al.* [19] where the TCF of LT has been reduced in the POI (−9.5 ppm/°C) by a factor of 4 with respect to the bulk (−39.6 ppm/°C). This enhancement is largely due to the addition of the above-mentioned SiO_2 layer that exhibits a positive TCF helping thus balancing the overall TCF of the stack around 0 ppm/°C [20]. Due to their heterogeneous nature, POIs are said to be dispersive substrates. This means that the working frequency of the substrate will be controlled by the thicknesses of the layers forming the stack, affecting consequently the wave's velocity of propagation. Owing to this property, the electromechanical coupling, the TCF as well as the gravimetric sensitivity will all depend on the chosen working frequency. In this paper, we divide the work into two major parts. The first part is theoretical and suggests the use of the POI substrates to evaluate the electromechanical coupling coefficients of the excited modes, assess their thermal stability through the TCF and finally estimate via simulations their gravimetric sensitivity. The second one aims at investigating the possibility of using substrates exciting modes with high electromechanical coupling coefficient [1] to replace the quartz substrate used in our original sensors. Accordingly, two SAW sensors have been selected for this study: a Rayleigh wave based on lithium niobate (128° Y-cut $LiNbO_3$) and a shear wave based on lithium tantalate (42° Y-cut $LiTaO_3$). The sensitivity of these sensors is compared with that of the Love wave based on the AT-cut quartz substrate. The gravimetric sensitivity of these sensors was studied numerically and the sensitivities of the fabricated sensors were estimated experimentally. The analysis takes into account all factors needed to serve the requirements imposed by the impaction system as well as the cleaning process.

2. Materials and methods

2.1. Cascade impactor

Our system is a customized cascade impactor [14] of three stages working at 3 Lpm flow rate in which two impaction plates have been replaced by SAW sensors. The first stage is equipped with an impaction plate for the collection of coarse particles with aerodynamic diameters higher than 10 μm. These particles are not measured since the toxicity of suspended particles is essentially due to particles with a diameter less than 10 μm. The last two stages are equipped with SAW sensors as impaction plates coupled with a monitor and aim at measuring and filtering the particles collected. The second stage will be measuring particles having a diameter between 2.5 and 10 μm. These particles will be referred to as PM10*. Although this nomenclature is not the conventional one used worldwide, it is still used in this paper to serve the purpose of highlighting the functioning mode of the impactor as well as the selectivity of its stages. For what concerns the third stage, it measures PM2.5 particles having a diameter less than 2.5 μm. A schematic representation can be seen in Fig. 3.

2.2. SAW sensors

SAW delay lines, used in this study, are based on piezoelectric substrates to generate waves at the surface. The quantification of particles is based on the gravimetric sensitivity. To overcome the perturbations due

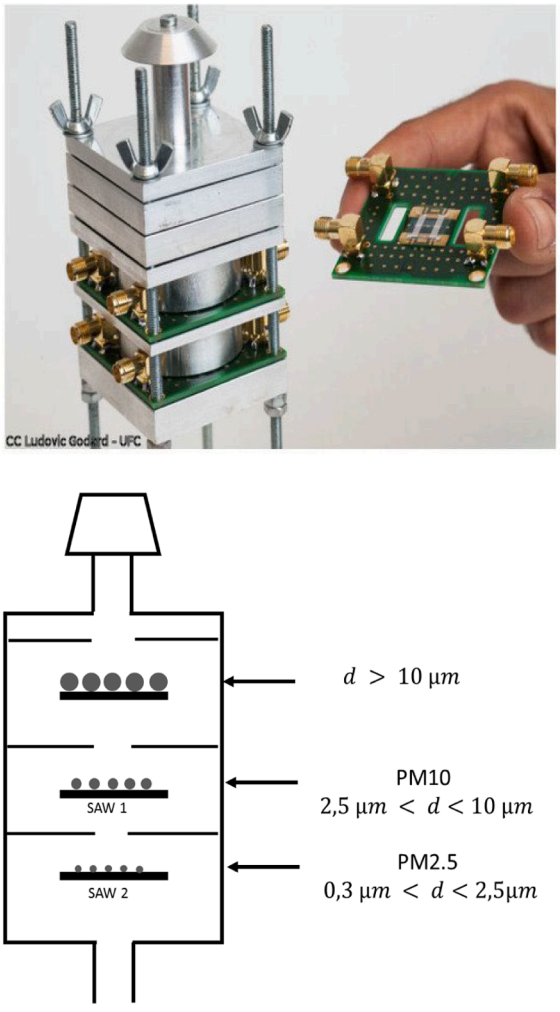

Fig. 3. A photograph (top) and a schematic figure (bottom) of our 3 Lpm cascade impactor [14].

to outer parameters such as temperature, pressure and humidity, a differential configuration relying on two delay lines was used. Each sensor is composed of two delay lines as shown in the zoomed part of Fig. 4. By positioning the holes of the impactor aligned with the sensing area of a specific delay line (the measurement line), the particles are collected only on this latter. The second one (the reference line) remains free of particles and is used as a reference. By subtracting the phase response of the reference line from that of the measurement line, we can accurately obtain the variation induced by the gravimetric effect as a result of PM deposition.

2.3. Fabrication process

The SAW sensors are composed of two InterDigitated Transducers (IDTs). The first one is used as an input and allows the generation of the acoustic wave while the second IDT enables the detection of the acoustic wave. The IDTs consist of double finger pairs of Aluminum with a thickness of 250 nm made by a lift off process. For sensors based on AT-cut quartz substrates, a silica guiding layer (1.5 μm) is necessary and was deposited on top of the IDTs using a PECVD process to allow the propagation of Love waves at the surface of the device. Similarly, for lithium niobate and tantalate substrates, delay lines are also designed by depositing comparable IDTs on their surface. To link the two ports of the delay line to the probing electronics, the electrical connection has to be opened using Deep Reactive Ion Etching (DRIE). The working frequency are 125 MHz, 100 MHz and 100 MHz, respectively, for sensors based on AT-cut quartz, 128° Y-cut $LiNbO_3$ and 41° Y-cut $LiNbO_3$.

2.4. Particle generation and experimental setup

In order to experimentally determine the sensitivity of the three sensors, a test bench has been developed as seen in Fig. 5. It enables us to generate particles with controlled concentrations. A particle generator AGK 2000 purchased from Palas® was used to produce fine particles from SiC solutions for PM10* and NaCl solutions for PM2.5 by nebulization. The size distribution and concentration of the generated particles depend on the concentration of the solution and the air pressure at the generator input. Therefore, the solutions were carefully calibrated and a digital pressure controller from Bronkhorst was coupled with the generator. An optical particle counter (OPC) FIDAS 100 ® was used as a reference system to measure the concentration inside the test chamber in order to correlate it with the measurements obtained from SAW sensors.

For particle sensing, the baseline phase of the SAW delay lines was stabilized under typical working conditions ($T \approx 25^{\circ}, RH \approx 30\%$). Then, the concentration in the chamber was stabilized around the targeted concentration. It was noticed that the particles generator produces the concentrations with a fluctuation of ± 20 $\mu g/m^3$.

3. Theoretical study: piezoelectric-on-insulator materials

3.1. Simulations

This part is established on the purpose of theoretically examining the tested substrates as well as evaluating innovative candidates for the sensing function of our impactor. Accordingly, this theoretical study aims at assessing the acoustic behavior of the POIs with different crystallographic orientations. In this case, we will evaluate those based on lithium tantalate (LT), which is already found commercially, and lithium niobate (LN) for comparative reasons. We start by building the stacked materials as shown in Fig. 6:

The piezoelectric substrates examined are, in accordance with IEEE standard, LT (YXl)/42° and (YXlt)/42°/90°, LN (YXl)/128° and (YXlt)/128°/90° and LN (YXl)/41° all five of them in their bulk form and POI forms. In the case of lithium niobate, a layer of 400 nm is mounted on 550 nm of SiO_2, as for lithium tantalate, a layer of 600 nm is mounted on 500 nm of SiO_2. These thicknesses are kept constant with the only variation being the crystallographic orientation of the piezoelectric layers. We would like to compare the acoustic behavior of the POI substrates to the bulk ones. We therefore focus on the electromechanical coupling coefficient (k^2), the temperature coefficient of frequency (TCF) as well as the gravimetric sensitivity (S). POI materials are heterogeneous structures as mentioned earlier, meaning that they possess a dispersive behavior which assumes a certain relationship between the working frequency and the wave's velocity. Consequently, the above-listed characteristics will all depend on the frequency at which the simulations are carried out. The simulations are done using a software developed by our team and make use of Green's function. This latter is better described as the impulse response of a medium upon an electric excitation or the application of a mechanical input on one of its surfaces [20]. The effective permittivity, which relates the charge distribution at the interface of two media to the electrical response of the medium considered, is then computed at the desired frequency. This is an essential parameter allowing the detection of the emerging modes. Based on that, the propagation velocity of the dominant modes is extracted. k^2 is next computed using the following equation:

$$k^2 = 2(v_f - v_m)/v_f$$

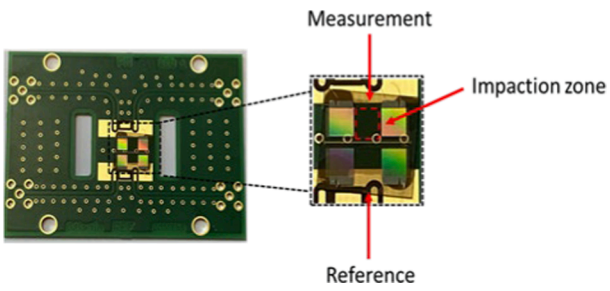

Fig. 4. A photograph of SAW sensors mounted on a PCB.

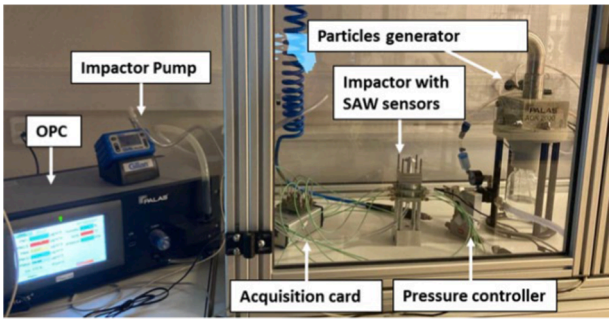

Fig. 5. The Experimental test bench for particles generation.

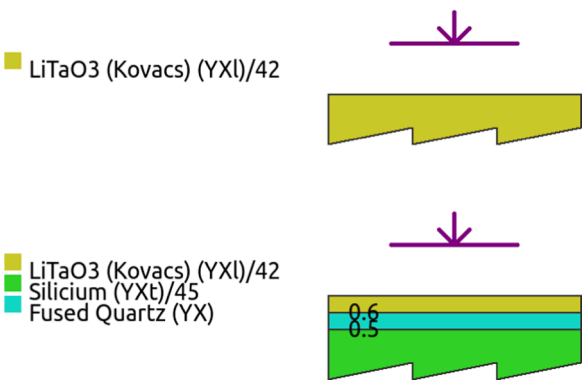

Fig. 6. Bulk (top) and stratified POI with 600 nm of LT42 and 500 nm of SiO_2 (bottom) lithium tantalate substrates.

where v_f is the free surface velocity and v_m is the metallized surface velocity.

Temperature-frequency drift of the sensors around their working frequency is also critical for its performance. It is assessed by calculating the TCF accounting for both the thermal expansion and the elastic properties of the material [19]. Using the following relationship, the impact of temperature on the frequency is determined:

$$F = F_0\left(1 + TCF_1.T + TCF_2.T^2 + TCF_3.T^3\right)$$

where $T = Temperature - T_0$ with $T_0 = 25\ ^\circ C$, $TCF_{1,2,3}$ are the first, second and third order temperature coefficients of frequency, F_0 is the central working frequency and F is the frequency affected by the temperature.

To predict the gravimetric sensitivity of the SAW sensors in question, a specific software developed in our team was used. It calculates the effective permittivity of a stratified medium from which we extract the propagation velocity of the existing modes as well as the coupling factor k^2.

A gold layer was used to mimic the mass of PM at the sensor's surface. Finally, the gravimetric sensitivity is calculated using the Sauerbrey approximation:

$$S_g = \frac{dv}{v_0}.\frac{A}{dm}$$

with $\frac{dv}{v_0}$ the relative shift in the speed of the wave, dm the mass variation and A the active surface of the sensor. In our case, the mass variation can be considered as the product of the density of gold ρ ($\rho = 19.3\ g/cm^3$), the surface considered in the model and the thickness of the gold layer de:

$dm = \rho\ de\ A$.

From there, the gravimetric sensitivity can be expressed as:

$$S_g = \frac{dv}{v_0}.\frac{1}{\rho de}$$

To begin with, the simulation results were used to estimate the expected sensitivity for the set of substrates we have in hand and for a set of POI substrates that we would like to assess for future optimization. The frequencies at which these simulations are done are chosen on the basis of the couple (TCF, k^2) where we have a good trade-off between a high k^2 and a low near zero TCF in absolute value. The sensitivity is then assessed for a range of thicknesses of the gold layer assimilating the mass loading effect owing to the deposition of particles on the sensor's surface. A 3D map can also be generated to detect visually the stability point and the frequency range ensuring the thermal stability required.

3.2. Simulation results and discussion

Recalling the fact that POI substrates have dispersive frequency-dependent behaviors, Fig. 7 shows the nonlinear relationship exhibited by the k^2 as a function of frequency for the substrates in their POI form. Over a range of frequencies from 200 to 2000 MHz, the LT42 (POI) for example presents superior k^2 values for high frequencies, primarily above 900 MHz. The maximum values of k^2 obtained are presented in Table 1.

Similarly, for the TCF, each substrate demonstrated to have a null TCF, each at its own frequency, presented in Table 2.

Since the frequencies at which the maximum k^2 value is different than that at which the TCF nullifies, the working frequency of our simulations is taken as a compromise between a TCF that is close enough to 0 and a k^2 that is high enough to guarantee a strong coupled mode that can be exploited later on for surface cleaning purposes. This choice relies on the fact that having a negligible TCF leads to a better sensitivity reading since influences imposed by temperature changes are overcome. Moreover, high k^2 values also ensure better coupling between particles and SAW, facilitating the cleaning process and enhancing the sensitivity. Based on these factors, POI substrates showed superior behavior with respect to their bulk forms for higher frequencies, making them optimal candidates for high frequency applications. Based on this analysis, Table 3 summarizes the frequency at which each substrate (in both forms bulk and POI) was simulated to assess its gravimetric sensitivity.

The behavior of the electromechanical coupling coefficient upon frequency variation is nonlinear and unpredictable without simulations. In some cases, it shows an increasing trend to a maximum value followed by a gradual drop.

As for the TCF, Fig. 8 also shows a nonlinear trend: increasing up to a certain frequency and decreasing beyond it. Each substrate shows thermal stability – where the TCF presents a null value – at its own working frequency as it is highlighted in Fig. 9 for the case of the POI

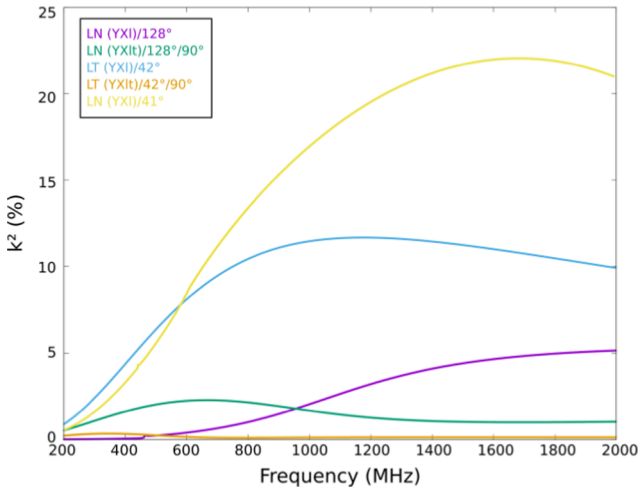

Fig. 7. The variation of the electromechanical coupling coefficient with the frequency for the considered substrates.

Table 1
Maximum k^2 values obtained for the substrates at different frequencies.

Substrate	Frequency (MHz)	k^2 (%)
LN128	2000	5.17
LN128/90	665	2.27
LN41	1700	22.01
LT42	1175	11.68
LT42/90	346	0.34

Table 2
Frequencies at which the TCF tends to zero for all four substrates.

Substrate	Frequency (MHz)
LN128	747
LN128/90	763
LN41	755
LT42	458
LT42/90	435

Table 3
Frequencies chosen for the simulations along with the obtained TCFs.

Substrate	Frequency (MHz)	TCF (ppm/°C)
LN128	800	6.73
LN128/90	760	−0.46
LN41	750	−0.74
LT42	500	3.21
LT42/90	400	−5.00

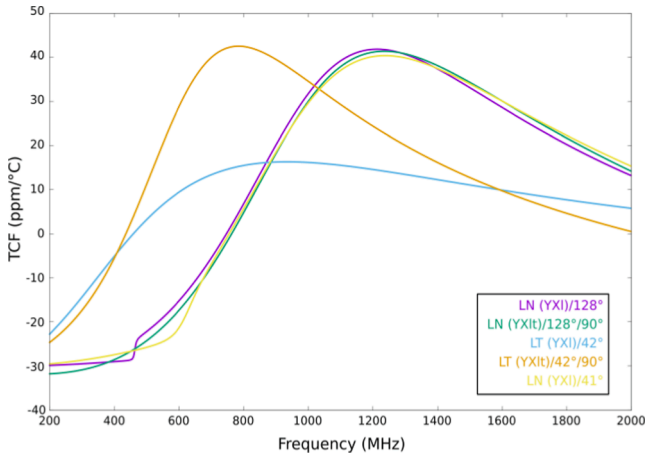

Fig. 8. Curves representing the temperature coefficient of frequency as a function of frequency.

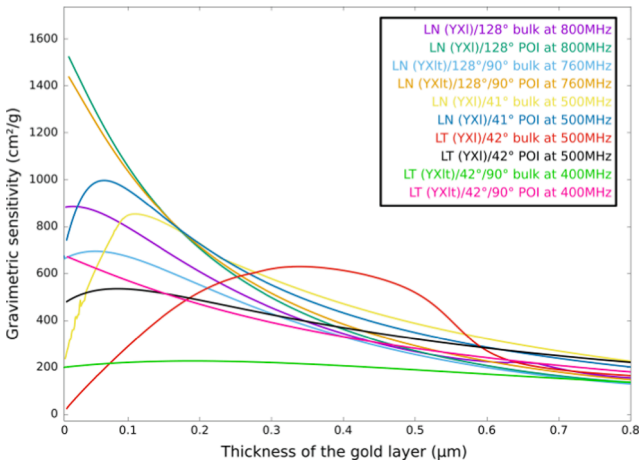

Fig. 10. The gravimetric sensitivity of the bulk and the POI substrates as a function of the thickness of the gold layer, each at its chosen frequency.

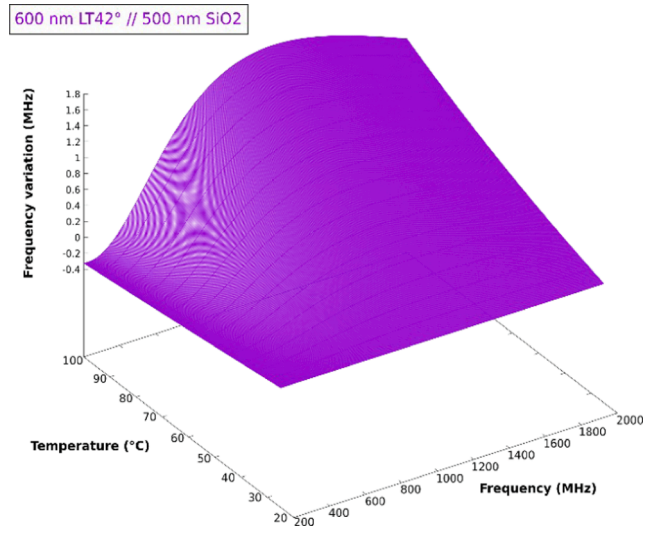

Fig. 9. The effect of the temperature on the frequency, studied for the lithium tantalate POI substrate. A stability point where negligible frequency variations are observed is detected for frequencies less than 700 MHz.

substrate with a configuration of 600 nm of LT (YXl)/42° on 500 nm of SiO_2.

The gravimetric sensitivity for the POI substrates is then estimated at the chosen frequencies. Fig. 10 presents the sensitivity curves with the gold layer thickness. POIs are observed to be more sensitive to the gold layer, i.e., the particle deposition, especially for thin layers. Both the POI and the bulk substrates display a continuous drip in their sensitivity as the gold layer thickens and then relatively stabilize exceeding a thickness of 300 nm of gold. Taking a closer look on LT 42° bulk, we notice multiple variations in the sensitivity with varying gold thicknesses. While taking LT 42°/90°, a stable sensitivity is noted among all thicknesses. Comparing the bulk curves with their POI, POIs exhibited higher sensitivities for thin gold layers. For thicker layers, all substrates showed similar trends converging towards close values. This is, in reality, attributed to the fact that the sensor loses its sensitivity upon its saturation with particles, from which the urge to couple our system with a cleaning feature.

Table 4 shows the improvement of the coupling coefficients as well as the temperature-frequency drift through a near zero TCF for all substrates considered except for LN128 where lowering the TCF was observed at the expense of the k^2. This result can be accepted or rejected

Table 4
Comparison of the simulated properties of the different materials in contrast with quartz, being the first substrate used in our impaction system.

Substrate		Frequency (MHz)	k^2 (%)	TCF (ppm/°C)
AT-Cut quartz		125	0.14	−0.035
LN128	Bulk	800	5.45	−75.0
	POI		1.00	6.73
LN128/90	Bulk	760	1.11	−83.0
	POI		2.20	−0.46
LN41	Bulk	750	15.44	−76.42
	POI		11.81	−0.74
LT42	Bulk	500	5.28	−26.53
	POI		6.36	3.21
LT42/90	Bulk	400	0.13	−40.8
	POI		0.32	−5.0

based on the application in question and its requisites. Moreover, and bearing in mind all results simultaneously, LN41 POI showed a significant improvement in the thermal stability and a slight decrease in the coupling coefficient with respect to the bulk form. These results make it as well a possible candidate as a substrate to our sensors fulfilling both requirements: sensing and surface cleaning.

It is also important to underline the fact that we can furthermore enhance these results by modifying the layers' thicknesses: that of the piezoelectric substrate and that of SiO_2 as the properties of this latter play a significant role in determining those of the stratified substrate as a whole. With that being said, adjusting the working frequency, the materials' thicknesses, the piezoelectric material crystallographic orientation and cut will all have significant impact on the properties being studied. Depending on the application and the desired characteristics, these mentioned parameters are carefully chosen. In our case and knowing that we are limited in terms of dimensions regarding our sensors, this imposes a constraint upon the working frequency. Theoretically, very high frequencies lead to miniaturizing the IDTs in a way that is not possible industrially. This also greatly reduces the PM sensing area affecting thus the precision and quality of the measurements.

4. Sensitivity characterization: experimental approach

In order to validate the theoretical approach towards the ability of the 3 sensors to detect fine particles in a lightly polluted environment, a monitoring of their phase at constant frequency, during successive exposures to particles, was performed. In this section, we report on the sensor's sensitivities obtained experimentally. Fig. 11 shows an example of the phase shift of sensor based on AT-cut quartz during successive exposures to particles.

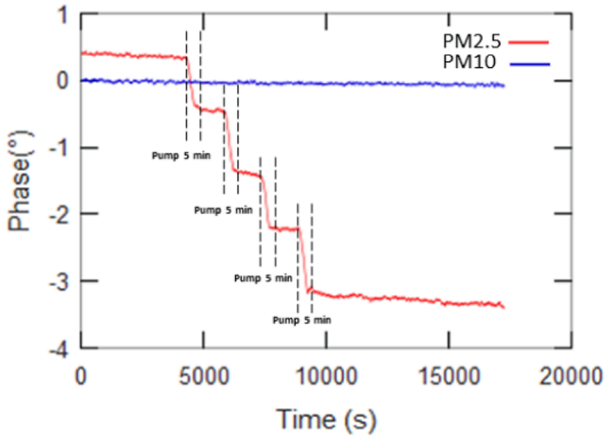

Fig. 11. SAW sensor phase shift of PM2.5 stage (red) and PM10* (blue) during successive exposures to particles in the [0, 2.5 μm] range.

In this case, only particles smaller than 2.5 μm were generated at a concentration of 150 μg/m^3. It can be seen that the curve of the PM10* stage does not show any measurable phase shift unlike that of the PM2.5 stage which shows a clear phase shift at each sampling. These results highlight the size separation efficiency of our impactor. The concentration is then obtained by determining the derivative of the phase variation during the particles sampling. In order to increase the accuracy, it is worth mentioning that 4 identical measurements were performed. The reported value is thus estimated by averaging these 4 measurements. Broadening our inspection to account for PM10*, this same measurement protocol was applied to all three sensors at different particles concentrations and by injecting particles with different sizes and generated with NaCl and SiC solutions. Thus, the absolute value of the phase derivative as a function of the particle concentration measured by FIDAS® optical system is presented in Fig. 12. A linear fit has been applied on the obtained curve to determine the sensitivity of the sensor.

From there, the sensitivity of the sensors has been determined. For Love wave-based sensors on AT-cut quartz substrates, the sensitivity was estimated to be 57°.s^{-1}.g^{-1}.m^3 for PM10* and 275°.s^{-1}.g^{-1}.m^3 for PM2.5. The Rayleigh wave-based sensors based on 128° Y-cut $LiNbO_3$ showed a sensitivity of 8°.s^{-1}.g^{-1}.m^3 for PM10* and 121°.s^{-1}.g^{-1}.m^3 for PM2.5 The PSAW sensors based on 41° Y-cut $LiNbO_3$ showed the lowest sensitivities among the tested sensors and are estimated to be 12°.s^{-1}.g^{-1}.m^3 for PM10* and 60°.s^{-1}.g^{-1}.m^3 for PM2.5 (Table 5 and Table 6).

We can notice that SAW sensors show different sensitivities toward PM10* and PM2.5. This can be due to the size and the different morphology of the particles. Particle size plays a crucial role in defining the sensor's response since most adhesion forces are linearly dependent on particle diameter [21]. Considering that smaller particles adhere more to the surface; the slowdown of the wave is more significant for PM2.5. The size-related sensitivity of SAW sensors was reported in a recent study [22]. In this latter, the higher sensitivity of SAW sensors toward PM2.5 can be explained by the fact that particles' coupling to the sensor's surface is dominated by the gravimetric effect for smaller particles and by the elastic effect for bigger particles. Although less sensitive than those of the Love wave sensor, the Rayleigh wave sensor based on 128° Y-cut $LiNbO_3$ remains a good candidate for PM measurement. On the other hand, the known phenomenon of rebound effect in cascade impactors may also explain the lower sensitivity toward PM10*. As outlined by Dahneke [23], a particle sticks to or rebounds from a substrate depending on the balance between the kinetic energy of the particle and other processes such as adhesion and the plastic deformation of the particle and/or the substrate.

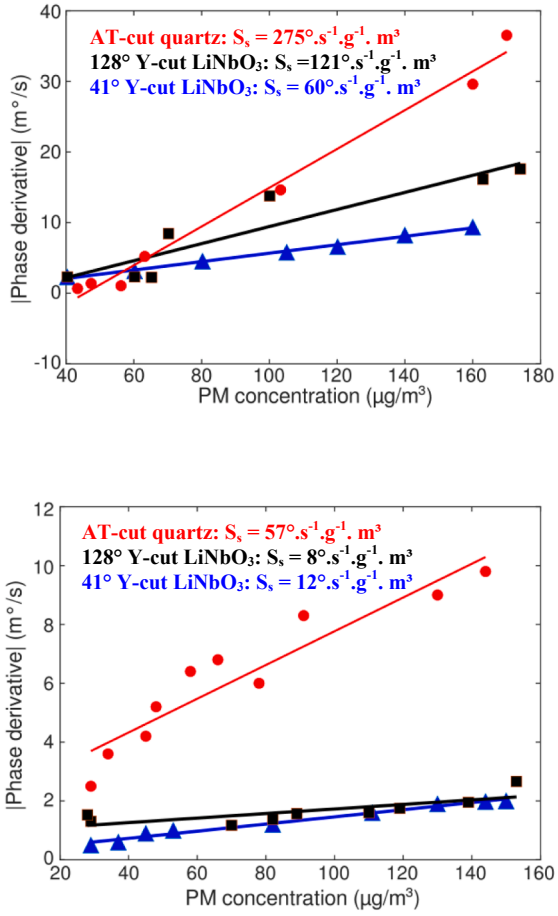

Fig. 12. Experimental characterization of the sensors sensitivity $S_{s,experimental}$ to PM2.5 (top) and to PM10* (bottom). (PM concentration measured by Fidas 100®).

Table 5
Experimental sensitivity to PM2.5 of sensors used in this study.

Sensor	S_s to PM2.5 (°.s^{-1}.g^{-1}.m^3)
AT-cut quartz (Love wave)	275
128° $LiNbO_3$ (Rayleigh wave)	121
41° $LiNbO_3$ (PSAW wave)	60

Table 6
Experimental sensitivity to PM10* of sensors used in this study.

Sensor	S_s to PM10* (°.s^{-1}.g^{-1}.m^3)
AT-cut quartz (Love wave)	57
128° $LiNbO_3$ (Rayleigh wave)	8
41° $LiNbO_3$ (PSAW wave)	12

5. Correlation of theoretical and experimental approaches

In an attempt to correlate the theoretical gravimetric sensitivities S_g obtained via simulations and the experimental sensor's sensitivities S_s, we developed the following relationship allowing to estimate the sensor's sensitivity. Starting again by Sauerbrey's equation:

$$S_g = \frac{df}{f_0}.\frac{A}{dm}$$

with dm representing the mass of particles deposited on the sensing area A as a function of the flow rate Q which is associated to the impactor's design. To define it, we should recall one essential hypothesis taken into consideration while designing the impactor. This hypothesis assumes a 50 % collection efficiency of the particles at each stage. In light of this, we can write the equation of dm as:

$$dm = \frac{1}{2} CQdt$$

with C being the PM concentration.

An additional equation is added to explain the phase-frequency relationship:

$$\alpha = \frac{d\varphi}{df}$$

Rearranging these equations, we deduce the equation of S_s as a function of S_g, α, f_0, Q and A:

$$S_{s,estimated} = S_g \frac{\alpha f_0 Q}{A}$$

with $S_{s,estimated} = \frac{1}{C} \cdot \frac{d\varphi}{dt}$ Applying this formula and using the simulated gravimetric sensitivities at the same frequencies at which each substrate was experimentally tested, we obtained the following results for the PM2.5 and PM10* stages:

Examining the values of the experimental and estimated sensitivities of the sensors in the last two columns of Table 7, we note two major observations:

i. The values of the estimated sensitivities remain unchanged regardless of the stage and the type of particles detected.
ii. The experimental sensitivities of all substrates and on both stages are significantly lower than the estimated ones.

This great discrepancy seen among the values is attributed to several factors that were not considered while deriving the correlation equation. On the basis of the first observation, it is discernible that the effect of the particles size, hence the stage at the which the sensors are mounted, does not appear in the equation since the estimated sensitivities are the same whether we are considering the stage measuring PM2.5 or PM10*. Moreover, particles tend to rebound off the surface depending on their nature and size. This phenomenon, in real cases, also affects the sensor's performance. We also need to highlight the complex interactions between the waves and the particles which is not accounted for in the equation. All these factors suggest the addition of an inevitable correction factor β to our equation such as $\beta < 1$ and is a function of:

i. The particles size and nature
ii. The waves-particles interactions, also depending on the type of waves
iii. The substrate-particles interactions (particle bounce effect)

Accordingly, it is possible to express the correlation equation as such:

$$S_{s,estimated} = S_g \frac{\alpha f_0 Q}{2A} \beta$$

Based on our data, the sensitivity to PM2.5 requires a $\beta < 0.25$, while to PM10* a $\beta < 0.05$. With certainty, these conditions cannot be generalized as extensive additional experiments and research are needed in order to validate and refine them. What we propose here is a simple model highlighting the complex relationship between the two sensitivities S_g and S_s.

6. conclusion and perspectives

In this research, we investigated an optimization plan to our impactor system aiming at measuring PM concentrations in the air using surface acoustic waves. This type of applications requires high electromechanical coupling and high thermal stability to ensure optimal working conditions serving the sensitivity to particles deposition. The original sensors were based on quartz substrates presenting a weak electromechanical coupling but a high thermal stability. To proceed with our optimization plan, a theoretical study based on simulations was carried out evaluating the possibility and feasibility of replacing the current substrates with innovative POIs. These stratified substrates proved their enhanced performance in regards of the electromechanical coupling and thermal stability at higher working frequencies with respect to their bulk forms. An experimental setup has then been considered to estimate the sensitivity of lithium niobate substrates. These sensitivities are subsequently compared to those of the AT-quartz based SAW sensors in the original system. The sensitivities of the selected devices were estimated against the presence of PM10* and PM2.5. In light of the simulated and experimental results, we demonstrated the potential of $LiNbO_3$ based SAW sensors to measure PM collected. Despite their lower sensitivity compared to AT-quartz based sensors, these sensors exhibit higher electromechanical coupling coefficient. This is important when developing next a self-cleaning system requiring displacing the particles off the sensing zone. Further investigations will be carried out to experimentally test the behavior of POI substrates. Furthermore, additional experiments are required to better define the correction factor imposed on the correlation model for the calculation of the sensor's sensitivity. This implies exploring different substrates of various cuts as well as a thorough analysis of the SAW-particles interactions, exploring particles of different size and nature.

Table 7
Experimental and estimated sensor's sensitivities to PM2.5 and PM10* at their respective stages.

Stage	Substrate	$S_{s,experimental}$ ($°.s^{-1}.g^{-1}.m^3$)	$S_{s,estimated}$ ($°.s^{-1}.g^{-1}.m^3$)
PM2.5	AT-cut quartz	275	1344
	128° $LiNbO_3$	121	562
	41° $LiNbO_3$	60	500
PM10*	AT-cut quartz	57	1344
	128° $LiNbO_3$	8	562
	41° $LiNbO_3$	12	500

CRediT authorship contribution statement

G. Fawaz: Writing – review & editing, Writing – original draft, Software, Methodology, Formal analysis, Data curation, Conceptualization. **FE. Dbibih:** Writing – original draft, Resources. **M. Vanotti:** Writing – review & editing, Validation, Software, Methodology, Conceptualization. **V. Soumann:** Resources, Methodology. **V. Blondeau-Patissier:** Writing – review & editing, Validation, Supervision, Project administration, Funding acquisition.

Declaration of competing interest

The authors declare the following financial interests/personal relationships which may be considered as potential competing interests: Ghida FAWAZ reports financial support was provided by Franche-Comté Electronics Mechanics Thermal Science and Optics Sciences and Technologies. Ghida FAWAZ reports a relationship with Franche-Comté Electronics Mechanics Thermal Science and Optics Sciences and Technologies that includes: employment. If there are other authors, they declare that they have no known competing financial interests or personal relationships that could have appeared to influence the work reported in this paper.

Data availability

The data that has been used is confidential.

Acknowledgment

This work was partly supported by the French RENATECH network and its FEMTO-ST technological facility as well as the Franche-Comté University.

References

[1] J. Bennès, S. Alzuaga, S. Ballandras, F. Chérioux, F. Bastien, et J. F. Manceau, « Droplet ejector using surface acoustic waves », in *Proceedings - IEEE Ultrasonics Symposium*, 2005, p. 823-826. doi: 10.1109/ULTSYM.2005.1602976.

[2] « Ambient (outdoor) air pollution ». Consulté le: 12 octobre 2021. [En ligne]. Disponible sur: https://www.who.int/news-room/fact-sheets/detail/ambient-(outdoor)-air-quality-and-health.

[3] C. Choirat, D. Ph, F. Dominici, D. Ph, J.D. Schwartz, D. Ph, Air pollution and mortality in the medicare population qian, N. Engl. J. Med. 376 (26) (2017) 2513–2522, https://doi.org/10.1056/NEJMoa1702747.

[4] J. Lelieveld, et al., Cardiovascular disease burden from ambient air pollution in Europe reassessed using novel hazard ratio functions, Eur. Heart J. 40 (20) (2019) 1590–1596, https://doi.org/10.1093/eurheartj/ehz135.

[5] A. Vodonos, Y.A. Awad, J. Schwartz, The concentration-response between long-term PM2.5 exposure and mortality; A meta-regression approach, Environ. Res. 166 (2018) 677–689, https://doi.org/10.1016/j.envres.2018.06.021.

[6] M. Franchini, C. Mengoli, M. Cruciani, C. Bonfanti, P.M. Mannucci, Association between particulate air pollution and venous thromboembolism: A systematic literature review, Eur. J. Intern. Med. 27 (2016) 10–13, https://doi.org/10.1016/j.ejim.2015.11.012.

[7] M. Vanotti *et al.*, Surface Acoustic Wave Sensors for the Detection of Hazardous Compounds in Indoor Air, in *Proceedings of Eurosensors 2017, Paris, France, 3–6 September 2017*, MDPI, 2017, p. 444. doi: 10.3390/proceedings1040444.

[8] J. Hornsteiner, E. Born, G. Fischerauer, et E. Riha, Surface acoustic wave sensors for high-temperature applications, in *Proceedings of the 1998 IEEE International Frequency Control Symposium (Cat. No.98CH36165)*, mai 1998, p. 615-620. doi: 10.1109/FREQ.1998.717964.

[9] R. Rimeika, D. Čiplys, V. Poderys, R. Rotomskis, M.S. Shur, Fast-response surface acoustic wave humidity sensor based on hematoporphyrin film, Sens. Actuators B Chem. 137 (2) (2009) 592–596, https://doi.org/10.1016/j.snb.2009.02.009.

[10] P. Sharma, K. Sreenivas, Highly sensitive ultraviolet detector based on ZnO/LiNbO3 hybrid surface acoustic wave filter, Appl. Phys. Lett. 83 (17) (2003) 3617–3619, https://doi.org/10.1063/1.1622436.

[11] N.W. Emanetoglu, J. Zhu, Y. Chen, J. Zhong, Y. Chen, Y. Lu, Surface acoustic wave ultraviolet photodetectors using epitaxial ZnO multilayers grown on r-plane sapphire, Appl. Phys. Lett. 85 (17) (2004) 3702–3704, https://doi.org/10.1063/1.1811383.

[12] W. Zhao, J. Liu, M. Liu, S. He, Research on a Surface acoustic wave based PM2.5 monitor, in: In *2019 IEEE International Ultrasonics Symposium (IUS)*, 2019, pp. 2557–2559, https://doi.org/10.1109/ULTSYM.2019.8926208.

[13] S. Thomas, M. Cole, F.H. Villa-López, J.W. Gardner, High frequency surface acoustic wave resonator-based sensor for particulate matter detection, Sens. Actuators Phys. 244 (2016) 138–145, https://doi.org/10.1016/j.sna.2016.04.003.

[14] L. Djoumi, M. Vanotti, V. Blondeau-Patissier, Real time cascade impactor based on surface acoustic wave delay lines for PM10 and PM2.5 mass concentration measurement, Sensors 18 (1) (2018), https://doi.org/10.3390/s18010255.

[15] V. Blondeau-Patissier *et al.*, Measurement of PM10 and PM2.5 from silicon carbide particles with cascade impactor based on Surface Acoustic Waves sensors », in *2019 5th Experiment International Conference (exp.at'19)*, 2019, p. 449-453. doi: 10.1109/EXPAT.2019.8876512.

[16] M. Paquit, et al., Displacement of Microparticles on Surface Acoustic Wave Delay Line Using High RF Power, in: In *2018 IEEE International Ultrasonics Symposium (IUS)*, 2018, pp. 1–4, https://doi.org/10.1109/ULTSYM.2018.8580122.

[17] P. Brunet, M. Baudoin, O.B. Matar, F. Zoueshtiagh, Droplet displacements and oscillations induced by ultrasonic surface acoustic waves: A quantitative study, Phys. Rev. E - Stat. Nonlinear Soft Matter Phys. 81 (3) (2010) 1–8, https://doi.org/10.1103/PhysRevE.81.036315.

[18] B. Aspar, et al., The generic nature of the Smart-Cut® process for thin film transfer, J. Electron. Mater. 30 (7) (2001) 834–840, https://doi.org/10.1007/s11664-001-0067-2.

[19] A. Clairet *et al.*, « New generation of composite substrates based on a layer of LiTaO3 on silicon for surface acoustic waves components », in *e-Forum Acusticum*, Lyon, France, 2020, p. 2527-2533. doi: 10.48465/fa.2020.0157.

[20] R. Ma, W. Liu, X. Sun, S. Zhou, et D. Lin, FEM Simulation of a High-Performance 128°Y–X LiNbO3/SiO2/Si Functional Substrate for Surface Acoustic Wave Gyroscopes, *Micromachines*, vol. 13, n° 2, 2022, doi: 10.3390/mi13020202.

[21] M.B. Ranade, Adhesion and removal of fine particles on surfaces, Aerosol Sci. Technol. 7 (2) (1987) 161–176, https://doi.org/10.1080/02786828708959155.

[22] J. Yang, J. Lu, Study of size-related sensitivity of surface acoustic wave sensor towards particulate matter sized particles using finite element and experimental methods, AIP Adv. 10 (2) (2020), https://doi.org/10.1063/1.5140066.

[23] B. Dahneke, The capture of aerosol particles by surfaces, J. Colloid Interface Sci. 37 (2) (1971) 342–353, https://doi.org/10.1016/0021-9797(71)90302-X.